

Hydrodynamics of photoionized columns in the Eagle Nebula, M 16

R.J.R. Williams, D. Ward-Thompson & A.P. Whitworth

Department of Physics and Astronomy, Cardiff University, PO Box 913, Cardiff CF24 3YB

Received **INSERT**; in original form **INSERT**

ABSTRACT

We present hydrodynamical simulations of the formation, structure and evolution of photoionized columns, with parameters based on those observed in the Eagle Nebula. On the basis of these simulations we argue that there is no unequivocal evidence that the dense neutral clumps at heads of the columns were cores in the pre-existing molecular cloud. In our simulations, a variety of initial conditions leads to the formation and maintenance of near-equilibrium columns. Therefore, it is likely that narrow columns will often occur in regions with large-scale inhomogeneities, but that observations of such columns can tell us little about the processes by which they formed. The manner in which the columns in our simulations develop suggests that their evolution may result in extended sequences of radiation-induced star formation.

Key words: ISM: clouds – H II regions – ISM: individual: M 16 (Eagle Nebula) – ISM: kinematics and dynamics

1 INTRODUCTION

H II regions are common features of regions of massive star formation, such as Orion or the Eagle Nebula, M 16, in which ultraviolet photons from young massive stars photoionize and photodissociate the molecular gas clouds from which the stars originally formed. Emission from the ionized gas, in lines such as the Balmer series or [O III] $\lambda 5007\text{\AA}$, allows the regions to be seen at optical wavelengths. Images of these regions have many different forms, although they may often be characterised as a photoevaporating blister.

The basic stratification of gas in an H II region is well understood. Close to the central star or stars the gas is highly ionized, as a result of the strong photoionizing continuum. Atoms which recombine within this region are rapidly photoionized once again, and the gas is maintained at an equilibrium temperature close to 10^4 K. At the edge of this region, where the photoionizing continuum spectrum has been essentially exhausted, is an ionization front (IF) which separates the ionized gas from atomic gas. The ionization front is generally narrow, compared to the overall scale of the region. Beyond the IF, the gas in the photodissociation region (PDR) is kept atomic by photons with wavelengths longer than 912\AA which do not have sufficient energy to ionize hydrogen, but are energetic enough to dissociate molecular hydrogen (Bertoldi & Draine 1996). Eventually, the spectrum of photodissociating photons is also absorbed, and the gas can remain molecular.

However, this simple stratification belies the intricate structures often observed in H II regions. A feature of par-

ticular interest is the photoionized columns, or ‘Elephant Trunks’, seen at the edges of regions such as M 16, M 20 and NGC 3603. These intrusions of molecular gas into the high-pressure environment of the ionized nebula are potentially important sites for star formation, and indeed evidence has been mounting which associates young stellar sources with the tips of the columns in M 16 (Hester et al. 1996; White et al. 1999). But the origin, structure and evolution of these columns has been the subject of controversy for many years. Do they result from pre-existing dense cores in the molecular gas or from instabilities in the IF/PDR structure? What is the timescale for their evolution?

1.1 The model of White et al.

White et al. (1999) have studied the structure of the columns in M 16 using observations in a wide variety of wavebands. They suggest that the heads of the columns are pre-existing molecular clumps which are now in the process of dynamical collapse, driven by an overpressure in the ionized gas around the heads, which will soon result in the formation of stars. In this model, gas at the heads of the columns in M 16 started to collapse at most 10^5 yr ago, when the ionization front (IF) moving away from the exciting stars reached their surfaces. The velocity of the shock driven into the neutral material by the IF is approximately

$$v_s \simeq \sqrt{\frac{P_{\text{sn}} - P_n}{\rho_n}} \quad (1)$$

where $P_{\text{sn}}/k_{\text{B}} \sim 1.2 \times 10^8 \text{ cm}^{-3} \text{ K}$ and $P_{\text{n}}/k_{\text{B}} \sim 3.5 \times 10^7 \text{ cm}^{-3} \text{ K}$ are the pressures inferred for the shocked neutral gas and for the gas at the head of the column, respectively, and $\rho_{\text{n}} \sim 2 \times 10^5 m_{\text{H}_2} \text{ cm}^{-3}$ is the density of the gas in the head. White et al. calculate that $v_{\text{s}} \simeq 1.5 \text{ km s}^{-1}$, and so that the shock will cross the head of the column in $\sim 1.5 \times 10^5 \text{ yr}$.

In consequence, White et al. argue that the columns have been subject to the incident radiation flux for a time no longer than this. For instance, the parameters given by White et al. imply that the flux of gas into the shock is $\sim 5 \times 10^{10} \text{ cm}^{-2} \text{ s}^{-1}$ H nuclei, while the mass flux out through the IF is $\sim 4 \times 10^9 \text{ cm}^{-2} \text{ s}^{-1}$ H nuclei. Even allowing for the different areas of IF and shock, shocked gas should pile up between them to a total column of $\sim 10^{23} \text{ cm}^{-2}$ in 10^5 yr . If the clump had been subject to photoevaporation for more than 10^5 yr , the shocked gas should now be observable in the CO or $850 \mu\text{m}$ data.

White et al. provide secondary support for the age they infer from detailed chemical and thermal modelling, which agrees with the observed properties of the molecular gas, and particular the low temperature of the densest molecular gas, and from the absence of diagnostics of protostars within the cold clumps. They argue that the distance between the ionization front and shock propagating into the clump will be far smaller than 0.2 pc , so the dense material seen at the head of the column cannot itself be shocked gas.

Based on this model, they propose that the tips of the columns in M 16 may represent the best examples known to date for earliest stages of Class 0 protostellar development, which have not yet collapsed far enough to obey the full criteria for Class 0 (André 1996).

1.2 Other possibilities

Despite the arguments of White et al. (1999), a lifetime of $\lesssim 10^5 \text{ yr}$ still seems difficult to reconcile with the dynamical age of the other structures around the columns. Since the density of the ionized gas around the column is far smaller than that of the molecular gas, the main ionization front is likely to be D-type. As a result, the IF and its leading shock will be moving into unperturbed molecular material ahead at a velocity $\lesssim 10 \text{ km s}^{-1}$. Indeed, since the age of the stellar cluster is $1-2 \times 10^6 \text{ yr}$, the average velocity of the ionization front over this lifetime can be no more than 2 km s^{-1} . Even if the velocity of the IF were as high as 10 km s^{-1} as it propagated along the sides of the column, the IF must have passed the head of the column at least $3 \times 10^4 \text{ yr}$ ago, so an age substantially smaller than 10^5 yr seems unlikely. Similarly, Hester et al. (1996) argue that the distribution of evaporating gaseous globules (EGGs) ahead of the column suggests that they are being photoevaporated on a timescale of a few $\times 10^4 \text{ yr}$ as the column recedes, so the limit on their distribution relies on this photoevaporation timescale rather than on the lifetime of the finger itself. Finally, the presence of strikingly similar columns in other regions suggests that columns may survive for a significant fraction of the total age of the H II regions into which they intrude. None of these arguments excludes the picture developed by White et al.; however, the upper and lower limits on the lifetime are tight, and may come to exclude it in time.

In the present paper, we will explore longer-lived alter-

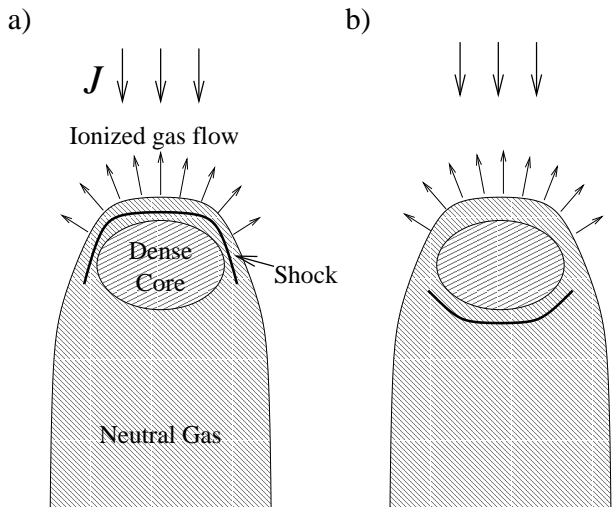


Figure 1. Schematic diagram of the Eagle columns, showing the possible positions of the ionization front and shock front. In both cases, the ionization front is coincident with the edge of the neutral material in the column, but in (a), the shock is between the ionization front and the dense molecular material in the head of the column as discussed by White et al. (1999), while in (b) it is between the head and the less dense molecular material in the barrel of the column.

natives to the model of White et al. One is that the dense gas in the head is separated from the lower density gas in the column by a shock. The comparison between this case and the model of White et al. is illustrated schematically in Figure 1. White et al. rule out such a scenario on the basis of the narrowness of the ionization front/shock front layer. Indeed, the predicted flux of H nuclei through the shock, $10^{10} \text{ cm}^{-2} \text{ s}^{-1}$, means that, to have collected the observed $30 M_{\odot}$ of gas in the head, it would have needed to propagate through approximately 1 pc of gas at the mean density of the neutral column over a timescale of $4 \times 10^5 \text{ yr}$: substantial fractions of both the size and lifetime of M 16. The collapse of the neutral material in the tangential direction may, however, decrease the time required to build up the mass (cf Bertoldi 1989). Structures of this form may result from density structures with initial contrast lower than those described by White et al., or from partial shadowing of the ionization front (Williams 1999). The detailed structures found in numerical hydrodynamic simulations below are more complex than those shown in Fig. 1, but accord broadly with this scenario.

Another alternative is that the dense gas at the head of the column is instead confined by gravity, with the shock leading the ionization front having effectively bypassed the region and moved away downstream. White et al. find that self-gravity may be important at the head of the column. The size of the region dominated by the gravity of the observed molecular core is about $\sim 0.13(M/30 M_{\odot})(\sigma/1 \text{ km s}^{-1})^{-2} \text{ pc}$, where $\sigma \simeq 1 \text{ km s}^{-1}$ is the effective sound speed of the gas (including contributions from turbulence and magnetic fields as well as the thermal sound speed) and $M \simeq 30 M_{\odot}$ is the mass of neutral gas in the head of the column.

In the following sections, we discuss numerical hydrodynamic simulations of these scenarios. These have been tai-

lored to the central column in M 16, which has the most symmetrical appearance and for which the observational data have the highest spatial resolution. We follow Hester et al.'s nomenclature, and term it column II (it is referred to as Π_2 by White et al.).

The structures which we find have some similarities to the equilibrium cometary cloud solutions discussed by Bertoldi & McKee (1990), based on the collapse of isolated, near-spherical clumps. However, our time-dependent hydrodynamical models give useful information on flow stability and the presence of shocks. Similar structures have been found by García-Segura & Franco (1996), in their study of the development of H II regions in inhomogeneous environments, although as a result of the global scope of their simulations individual columns were poorly resolved. Mellemma et al. (1998) model the formation of neutral tails behind isolated dense clumps in some detail. The models we present here have been developed for cases where the columns are close to the edge of an H II region, with parameters chosen to compare directly with those in M 16.

In Section 2, we discuss the derivation of suitable parameters for our numerical models from the observational data, and particularly the comparison of the pressures of ionized and neutral gas across the ionization front at the head of the column. In particular, we find that the observational evidence for an overpressure around the heads is weak. In Section 3, we discuss the numerical method we have used, and, in Section 4, the initial conditions for the simulations. In Section 5, we present the results of these simulations, and in Section 6 discuss their implications.

2 THE COLUMNS IN THE EAGLE NEBULA, M 16

2.1 Observational data

The columns in M 16 have been studied by many authors. Perhaps the best optical data is the HST narrow band imaging of Hester et al. (1996). We retrieved two $\text{H}\alpha$ images from this data set from the HST archive, and stacked and median-limited them to remove strong cosmic ray features and very fine-scale structures. The resulting image is shown in Figure 2. There are many striking irregularities in this image. Small clumps break the surface, and some appear fully separated from it. Close to the apex, the surface is puckered on a fine scale. Some of the clumps harbour K-band sources, and are identified as protostars by Hester et al. Away from the head, the surface irregularities seem to grow in width, with bright regions where their surfaces face towards the source of ionization. In addition, we note the low-magnitude striations which are seen along lines approximately perpendicular to the nearest surface.

White et al. (1999) combined this optical data with observations of M 16 in molecular lines, millimetre and sub-millimetre continuum and the mid-infrared, to present a remarkably complete picture of properties of the gas and dust in and around the columns. Within the columns, molecular gas is probed by line emission and the associated dust is seen in millimetre/sub-mm emission, while $\text{H}\alpha$ and radio continuum observations are sensitive to structures in the surrounding ionized gas.

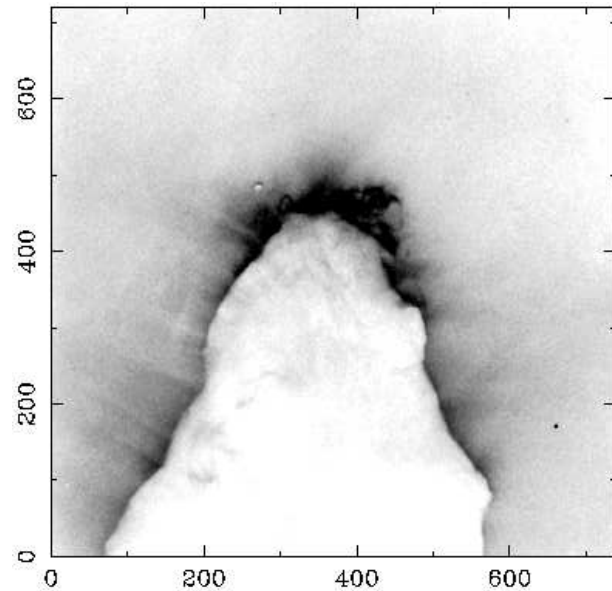


Figure 2. Cleaned $\text{H}\alpha$ image, shown negative and with a grayscale saturated in order to bring out low contrast features. The axes are labelled in pixels, where each pixel corresponds to $1.4 \times 10^{15} \text{ cm}$, for Hester et al.'s adopted distance of 2 kpc.

Levenson et al. (2000) have observed excited H_2 emission in M 16, to study the properties of the PDR which leads the ionization front. They find that their observations are consistent with a stationary photodissociation region, around $2 \times 10^{17} \text{ cm}$ deep (although since the properties of the incident radiation field are not well determined, it is possible that shocks driven by the IF might also contribute to the collisional component of this emission).

2.2 Comparison with photoevaporated winds

In Figure 3, we show cuts through this image. The first is along the axis of the large-scale column which is vertical in Fig. 2. The values are averages for a strip between 345 and 355 on the x -axis. The second is perpendicular to this, averaged for a strip between 395 and 405 on the y -axis.

In Fig. 4, we show the radial emission measure profile derived from isothermal wind models, as described by Henneny & Arthur (1998). These authors found that such models gave a very good fit to $\text{H}\alpha$ emission profiles of gas photoevaporated from proplyds in the Orion nebula. We have here been rather less strenuous in the correction of the observational data for contamination by continuum and $[\text{N II}]$ emission, but our aim in this section is simply to get an indication of the properties which pertain at the head of column II.

Comparing the model profiles with Fig. 3, we see that their overall forms are very similar. The central brightness of the columns appears rather lower, relative to that at large distances, than the model would predict, but that may be explained by the decreasing intensity of illumination as the surface of the column points away from the head and by the occulting of background emission by the column. The sharpness of the inner edge of the profile suggests that the column is slightly closer to us than is the photoionizing star.

More fundamentally, if (following Hester et al.) we take the radius of curvature of the head of the column to be

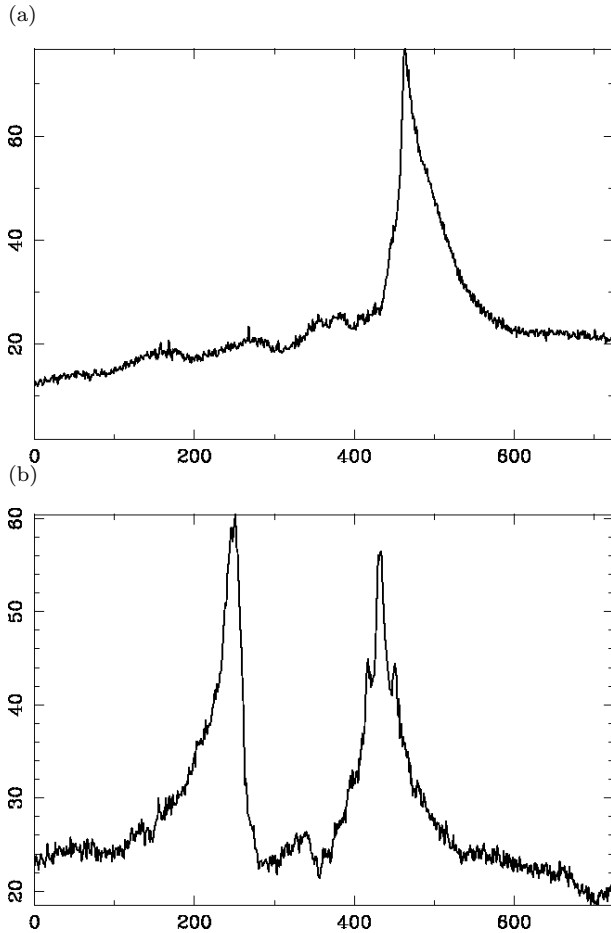


Figure 3. Sections through the data (a) top-to-bottom (b) left-to-right.

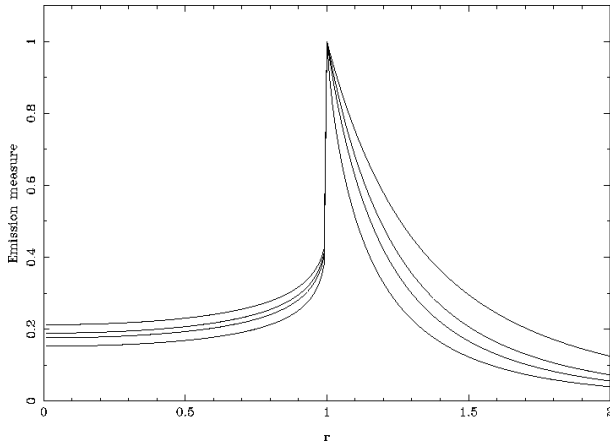


Figure 4. Sections through spherical flow models for isothermal winds which start from Mach 1, 1.2 and 2 at the surface of the column, and for constant velocity flow. The plots have been normalized to fixed peak emission measure: the sharpest plot is for a Mach 1 outflow while the smoothest is for constant velocity outflow.

90 pixels, then the breadth of the observed H α profile is difficult to account for. Not even the most extreme of the models in Figure 4 explains the width of the transverse light distribution. For comparison, Sankrit & Hester (2000) find that power-law models with a radius of curvature of 2×10^{17} cm \simeq 150 pixels fit the emission profile in several emission lines, which confirms that the effective radius of curvature is larger than that apparent in the images. Megeath & Wilson (1997) also find that the radio emission measure is more extended in their observations of photoevaporating clumps in NGC 281 West than for a $n_e \propto 1/r^2$ density model.

One possible explanation for the M 16 results is that the head of the observed column is more elongated along the line of sight than perpendicular to it. Alternatively, if the column is directed into the plane of the sky (Pound 1998), the inner peak of the emission measure profile may be hidden from view, although the inclination does not appear to be that extreme.

2.3 Inferred density and radiation field

For the model ionized flow profiles, isothermal flow with initial Mach numbers of 1, 1.2, 2 and constant velocity flow, the effective integration distance (i.e. the peak emission measure divided by the square of the peak density) is 0.8, 1.0, 1.3, and $\pi/2$ times the radius of curvature, respectively. This may be compared to the value of one-half assumed by Hester et al. (since the profiles are well resolved, the correction due to resolution effects is minimal). When the uncertainty in the local radius of curvature is included, it seems very likely that Hester et al.'s value of 4000 cm^{-3} for the electron density at the head of column II may have been overestimated. Indeed, Hester et al.'s own photoionization modelling suggested that the density at the head of the column is 2000 cm^{-3} (although this has subsequently been revised by Sankrit & Hester 2000). As a result, the ionized gas may not in fact have a greater pressure than the effective pressure in the neutral gas at the head of the column.

The density at the head of the column can also be used to determine the incident ionizing flux. The thickness parallel to the radiation field is roughly $\ell \sim 0.04 \text{ pc}$ from Figure 3. Balancing the number of recombinations in the flow with the intensity of the incident ionizing radiation, J , suggests that $J \sim \alpha_B n_e^2 l \simeq 1.3 \times 10^{11} \text{ cm}^{-2} \text{ s}^{-1}$, for a peak electron density of $n_e \sim 2000 \text{ cm}^{-3}$. It is difficult to follow White et al.'s analysis of their VLA data, but assuming that the integrated 48 mJy emission corresponds to that occulted by the head of the column, which has a radius of curvature of 0.04 pc (Hester et al. 1996), the incident ionizing intensity predicted by the formulae of Lefloch, Lazareff & Castets (1997) is $J \sim 1.5 \times 10^{11} \text{ cm}^{-2} \text{ s}^{-1}$. These values are mutually consistent, but smaller than those found by White et al., and also smaller than the values, inferred from stellar censuses, of $4.4 \times 10^{11} \text{ cm}^{-2} \text{ s}^{-1}$ (Hester et al. 1996) or $2.6 \times 10^{11} \text{ cm}^{-2} \text{ s}^{-1}$ (from the total flux given by Pound 1998). However, this difference can easily be accounted for by uncertainties in the ionizing flux of the stars, as the result of dust absorption or photoionization between the ionizing stars and the columns, or by the geometry of the region.

In our models, we neglect the role which a PDR may have in the dynamics of the region. The depth of the PDR

in M 16, as derived by Levenson et al. (2000), is close to the radius of curvature of the finger tips, so this assumption is only marginally valid. However, since the column density inferred is close to the stationary models (rather than being substantially affected by advection, cf. Bertoldi & Draine 1996), it seems likely that the jump conditions across the combined IF/PDR structure are determined principally by the flux incident on the IF.*

2.4 Derived parameters

Based on the observations, we will adopt the following parameters for our modelling of column II. The pressure in the ionized gas at the head of the clump is $P_i/k_B \simeq 3 \times 10^7 \text{ cm}^{-3} \text{ K}$; this ionized gas is assumed to have an isothermal sound speed of 10 km s^{-1} . The density in the molecular gas in the core at the head is $n(\text{H}_2) = 2 \times 10^5 \text{ cm}^{-3}$ while that in the column of gas behind is typically 10 times smaller than this. White et al. suggest that while the temperature of the gas is 20 K throughout the column, the effective pressure within the columns is dominated by the effects of small-scale magnetic fields and turbulence, as evidenced by the smooth profiles of molecular lines with widths $\sim 2 \text{ km s}^{-1}$. We cater for this in our dynamical models by assuming that the neutral gas behaves as if it were isothermal with a temperature of 200 K (note that the turbulent contribution to the pressure in the molecular gas also reduces the importance of heating in the PDR for dynamical modelling). The total mass in the core of column II is 31 M_\odot and its radius is 0.085 pc. We assume a photoionizing flux of $10^{11} \text{ cm}^{-2} \text{ s}^{-1}$, impinging on the column parallel to its axis.

3 NUMERICAL METHOD AND ASSUMPTIONS

We use the hydrodynamical code described by Williams (1999), which is based on the second-order Godunov algorithm by Falle (1991). Ionization and recombination are treated by including the equations

$$n \frac{dx}{dt} = an(1-x)J - \alpha_B n^2 x^2 \quad (2)$$

$$\frac{dJ}{dz} = -an(1-x)J. \quad (3)$$

Here n is the density of hydrogen nucleons, x the ionization fraction and J is the number flux of ionizing photons, assumed to propagate parallel to the z axis. The photoionization cross-section of hydrogen, a , and the case B recombination coefficient, α_B , are taken as constants. The electron density, nx , is included as an advected variable in the hydrodynamic solver, and the ionization and recombination equations included by operator-splitting, implemented at the end of each step (and also for the intervening half-steps). The

* If, in other cases, the depth of a PDR in pressure equilibrium with the photoionized flow were larger than the radius of a globule, the PDR would be important in development of the globule; if it were larger than the inter-globule separation, the development of photoionized columns might be suppressed, with the internal structure of the molecular cloud only observable in atomic and molecular species.

equations are integrated using an implicit scheme to advance x in time and J across each grid cell.

The code does not include a treatment of the diffuse ionizing radiation field (beyond using the case-B recombination coefficient). In the on-the-spot approximation, the diffuse field is found to be ~ 15 per cent of the *local* direct radiation field (Cantó et al. 1998). The characteristic length for reabsorption of diffuse photons is $\ell \sim J/\alpha_B n^2 \simeq 0.05 \text{ pc}$ (dependent, or course, on spatial variations of J and n), so the diffuse field might be expected to have some effect even on structures as large as the columns. More detailed treatments predict that the diffuse radiation is a smaller fraction of the direct field away from the edge of the global photoionized region (Rubin 1968). Close to the edge, where relative size of the diffuse field is larger, the soft spectrum of the diffuse field will result in a smaller path length to absorption than for the direct field. The low contrast of the surfaces of the observed columns which do not point towards the ionizing source is empirical evidence that the diffuse radiation field would be adequately treated by the on-the-spot approximation in the present case.

Since the internal structures of IFs are not resolved in the simulations, most of the gas will be either almost completely ionized or fully neutral. Intervening regions with intermediate ionization are likely to result principally from numerical mixing, so physically detailed schemes which assume the gas within the computational cells is reasonably uniform are not appropriate. Instead, we set isothermal sound speed in the gas to

$$c_s = (1 + 99x)^{1/2} \text{ km s}^{-1}. \quad (4)$$

This expression results from assuming that in cells with $0 < x < 1$, the gas is split into separate regions of fully ionized and fully neutral gas, in pressure equilibrium with each other, and so gives a better account of the sub-grid structure at the (dynamically significant) D-type IF.

4 INITIAL AND BOUNDARY CONDITIONS

The main model presented here is calculated in cylindrical symmetry, with coordinates (r, z) . A uniform 128×448 grid covers physical dimensions $0 < r < 0.5 \text{ pc}$ and $0 < z < 1.75 \text{ pc}$. The boundary conditions are reflective on the axis, $r = 0$, as required by symmetry. On the boundary towards the source, $z = 1.75 \text{ pc}$, free-flow boundary conditions are used when the flow is outwards, mirror conditions when it is inwards, although as the outward flow is generally supersonic this has little influence on the flow inside the grid. Along the outer radial boundary, $r = 0.5 \text{ pc}$, the conditions beyond the grid are either free-outflow/zero-inflow if the ionization fraction is larger than 0.1, or mirror conditions if it is less than this value. This somewhat artificial criterion changes the behaviour at the boundary at the IF, in order to model an ionized flow which is divergent on large scales. The effect depends little on the specific limiting value, as away from the IF the gas is in general either almost entirely ionized or almost entirely neutral.

On the edge of the grid towards the molecular cloud, $z = 0$, the boundary condition is set by assuming that the material retains its initial state, i.e. in most of our examples a flow of gas towards the IF. As the solution develops,

a shock often becomes captured at the boundary, which reduces the inflow speed and increases the inflow density. The flux of neutral gas into the grid through the plane $z = 0$ is, in all cases, small enough that it could not prevent the IF from entering if the entire grid were full of neutral material. In many cases, the density of the ionized gas becomes large enough to absorb all the ionizing photons within the size of the grid. Where the ‘molecular’ boundary covers the entire upstream edge of the grid, a plane-parallel IF is an equilibrium solution. If the ionized flow is allowed to escape from the side of the region, it is not obvious what the form of the equilibrium will be, if indeed there is one. One possibility is that the IF surface will remain smooth, and a steady solution will be found in which the variation in pressure at the IF is balanced by changes in flow velocity via the Bernoulli effect.

However, these IF are believed to be unstable to corrugation modes on both small and large scales, although for wavelengths larger than $6 \times 10^{15} n_3^{-1}$ cm recombination decreases the growth rate of these instabilities decreases rapidly (Kahn 1958; Axford 1964; Sysoev 1997). This wavelength is comparable to our grid scale of 10^{16} cm for typical ionized gas densities at the IF of $\sim 10^3$ cm $^{-3}$. We now present numerical models which illustrate what may happen for a range of initial conditions.

The models we have calculated have initial conditions split into two regions: ionized gas with a density $n(\text{H total}) = 200$ cm $^{-3}$ towards the source of ionizing photons and moving towards it at 10 km s $^{-1}$ relative to the neutral gas behind. This neutral gas has density, $n(\text{H total}) = 2 \times 10^4$ cm $^{-3}$ (n.b., not $n(\text{H}_2)$, see below). Except where noted, in the initial conditions the neutral gas is assumed to move at 2 km s $^{-1}$ towards the ionizing source in order to keep the ionization front broadly at rest within the grid, with the ionized gas assumed to stream towards the radiation source 10 km s $^{-1}$ more rapidly than this. Pressure equilibrium holds where ionized and neutral gas are alongside each other. We take the ionizing flux incident at the top of the grid in the figures to be 1.5×10^{11} cm $^{-2}$ s $^{-1}$, since recombinations in the upstream flow are found to reduce the ionizing radiation incident on the head of the column somewhat. The Strömgren distance in the ionized gas, ~ 3 pc, is sufficiently great that a column the length of the computational grid can be maintained with almost complete ionization for the initial conditions.

The boundary between these regions is assumed either to be plane (to study the development for small perturbations) or to include a column of dense gas (to study the likely long-timescale development of the columns observed in many regions).

5 RESULTS

We will now present the results of four different scenarios for the development of photoevaporated columns.

Case I is based on the model of White et al. (1999), including initial density stratification and gravity,

Case II has an initial short cylindrical column,

Case III has a 10 per cent deficit in photoionizing flux close to the axis,

Case IV has dense neutral gas initially filling the grid, with gravitational forces from a $30 M_\odot$ object included.

Case I: In Figure 5, we present the results of a first simulation in which the flow conditions modelled on those inferred by White et al. The initial conditions have a dense core of material at the head, and a lower density column behind. A gravitational potential from a $30 M_\odot$ mass, smoothed at a radius of 0.08 pc, is centred on the core of the head. The uniform gas at the head of the column initially falls in, as it is not in equilibrium with the gravitational field, but does not collapse far because of the smoothed core of the field.

By the time of the second frame, 10^5 yr after the start of the simulation, the shock at the head of the column has passed through much of the dense gas. The shock proceeds down the column in later frames. Soon the ram pressure of the radiation field is sufficient to push the dense gas away from the gravitating core. The amount of gas with density above 10^5 cm $^{-3}$ in these models remains roughly constant, and so the gravitational field would in reality respond to this movement. Nevertheless, it is striking that the density field in the column remains close to that inferred by White et al. even when the head is a considerable distance away from the gravitating centre, rather than requiring the head of the column to be caught within 10^5 yr after the IF reaches it.

In the remaining examples, we investigate possibilities by which such structures may have formed, and what conditions are necessary for them to be long-lived.

Case II: In Figure 6, we illustrate a case in which a short column of gas is initially present. The radius of the column is initially 0.125 pc and it stands proud by 0.5 pc ahead of the main body of molecular material. The column is again seen to be long lived, but highly variable. Certain broad features characterise the structure. The highest densities in the neutral gas are seen close to the head of the column, and reach values similar to those inferred for the column tip by White et al.

The surface of the column is convoluted. Neutral clumps split off from the column at different stages (e.g. close to the base of the column in Figure 6f) and linear structures are seen where different streams of ionized gas interact. These are reminiscent of the observed clumps and striations in the flow (see Figure 2 and Section 2). The striations are sometimes seen to be triggered by surface inhomogeneities resulting from the discrete nature of the grid. However, the growth of these instabilities appears to be a generic feature of the development of obliquely-illuminated ionization fronts (Vandervoort 1962), even when account is taken of the effects of recombination in the upstream flow (Williams, in preparation).

In the frames shown in Figure 6, the dense column becomes more marked with time. Initially, the ionizing field generates a strong flow away from the head of the column, a low density region ahead of it and a net acceleration away from the ionizing source (the well-known ‘rocket effect’, Oort & Spitzer 1954). However, we see here that short lengthscale which characterises the photoevaporative flow from the head means that its pressure decreases rapidly, and eventually a termination shock forms. The convergence of this termination shock at the axis leads to the formation of an over-dense region at larger distances from the column. Such over-dense regions lead to the formation of some thin filaments connected to the main ionization front [e.g., those seen close to

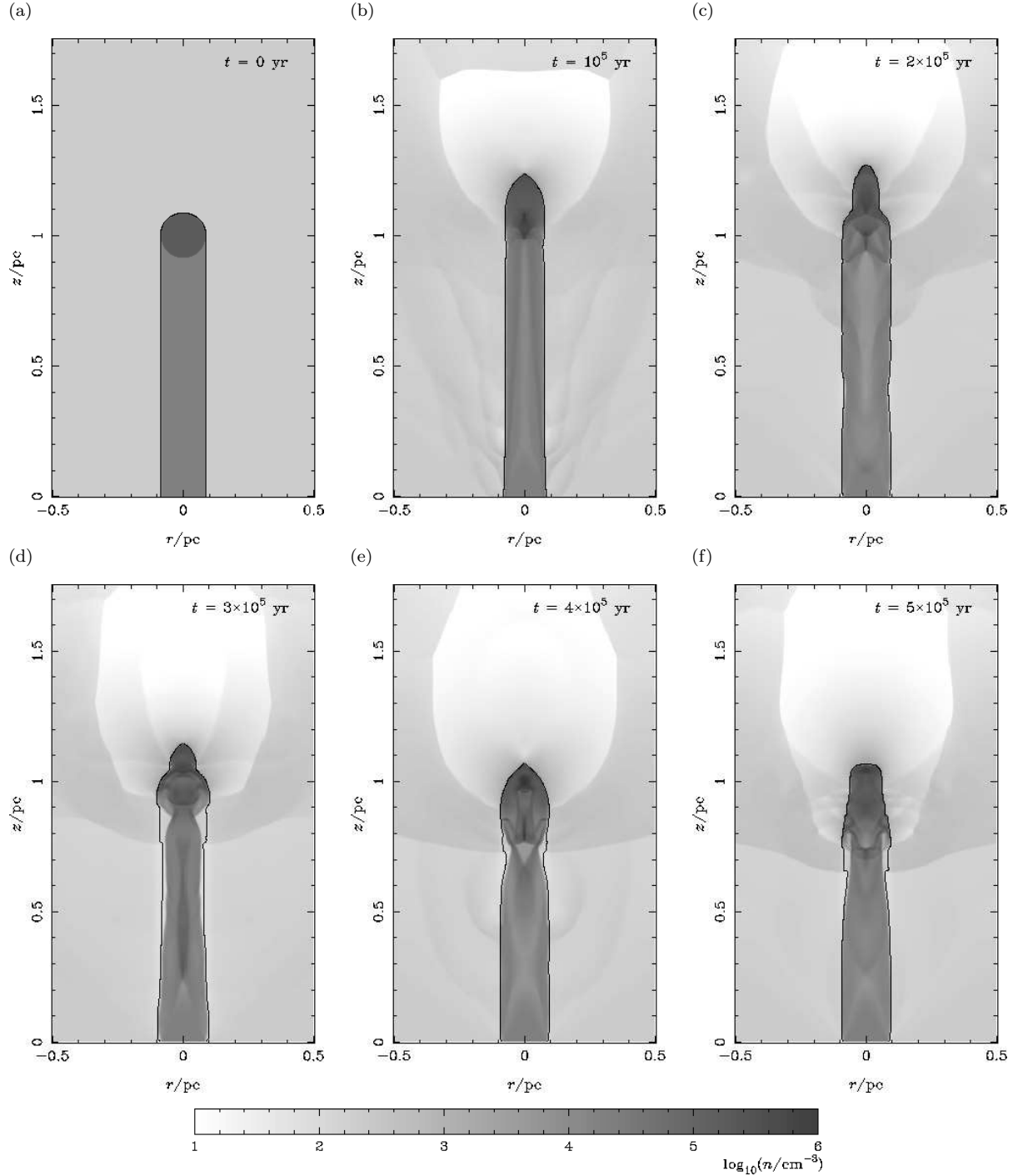


Figure 5. Greyscale plots of log density for Case I: an initial column of gas based on the model of White et al. The plots are shown at the labelled times after the start of the simulation. The density range calibration is shown in the colour bar; a single contour marks the location of the ionization front.

the base of the column in Figure 6(b)]. Filaments at the head of the column can allow the column to move forward once again, although the rigidity provided for the filaments by the reflecting boundary condition on-axis may have a significant influence by preventing non-axisymmetric instability modes.

Case III: In Figure 7, we show the development of columns for a case where there is a 10 per cent weakening

of the impinging ionizing radiation field for a small radius around the axis. A narrow feature in the radiation field such as this might form by an upstream overdensity: a photo-evaporating globule, for instance, or dense structures close to the stars caused by interacting stellar winds.

A strong column soon forms in this case. Once it has formed, its evolution is not greatly influenced by the small perturbation in the radiation field. The structure is broadly similar to those seen in the previous two cases, although the

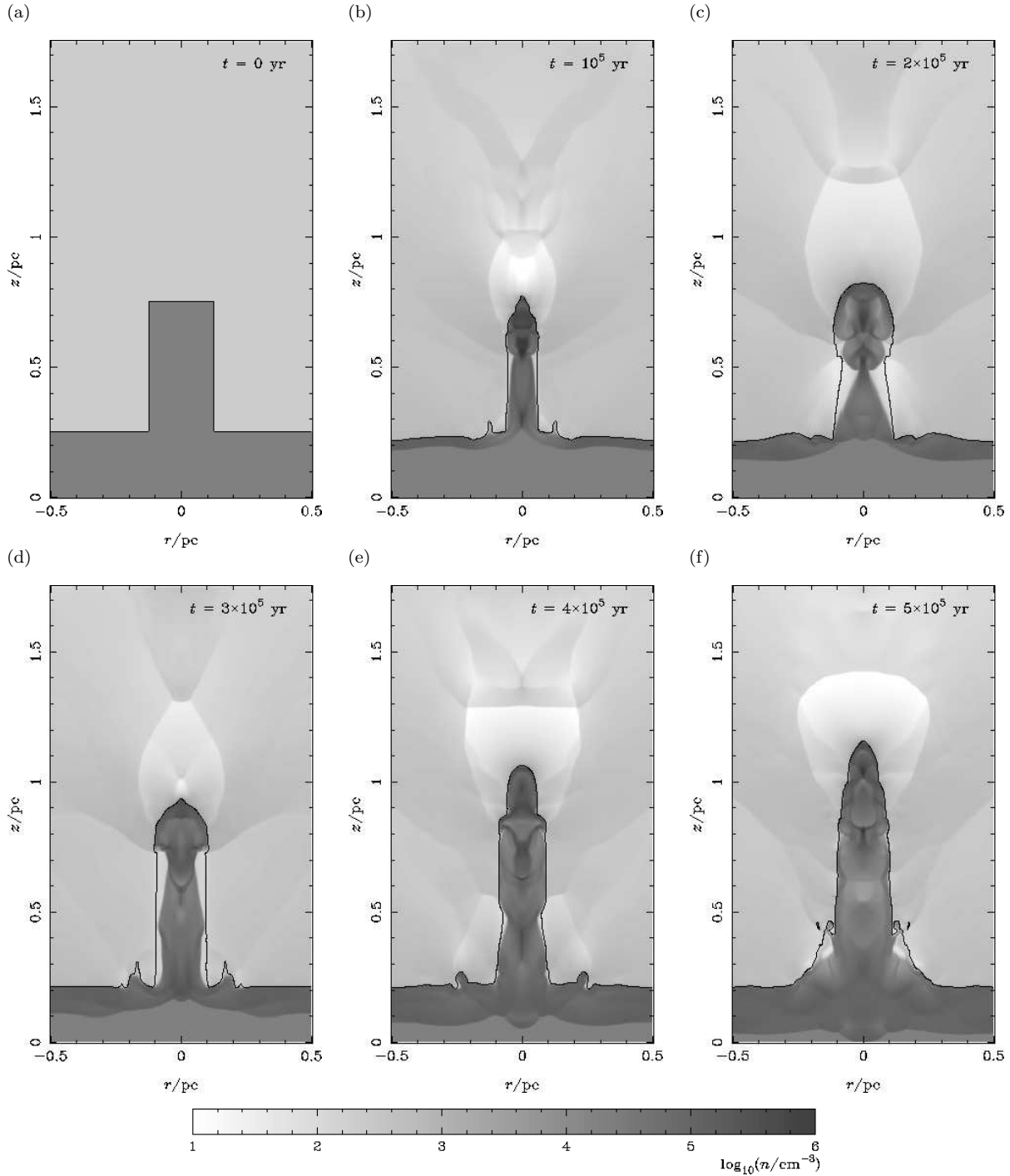


Figure 6. Greyscale plots of log density for Case II. The plots are shown at (a) initial time (b) 10^5 yr, (c) 2×10^5 yr, (d) 3×10^5 yr, (e) 4×10^5 yr, and (f) 5×10^5 yr after the start of the simulation. The full density range is typically from 3 to 10^6 cm^{-3} , although the gas which fills most of the volume of the column is between 5×10^4 and $5 \times 10^5 \text{ cm}^{-3}$.

column has a somewhat higher aspect ratio and the shock remains within the computational grid for a longer period.

Case IV: In Figure 8, we take uniform dense gas to nearly fill the grid, and include a gravitational field equivalent to a 30-M_\odot core smoothed at a radius of 0.02 pc . In this case only, the neutral gas is initially at rest. As the simulation develops, mass first falls into the gravitational

potential, to form a dense core close to hydrostatic equilibrium. A shock and ionization front driven by the impinging ionizing radiation propagate over this core, generating a column structure. This column is very long-lived, tending to form a cometary structure at late times. The length of this cometary structure may in reality be limited by the non-plane parallel ionizing radiation field resulting from dif-

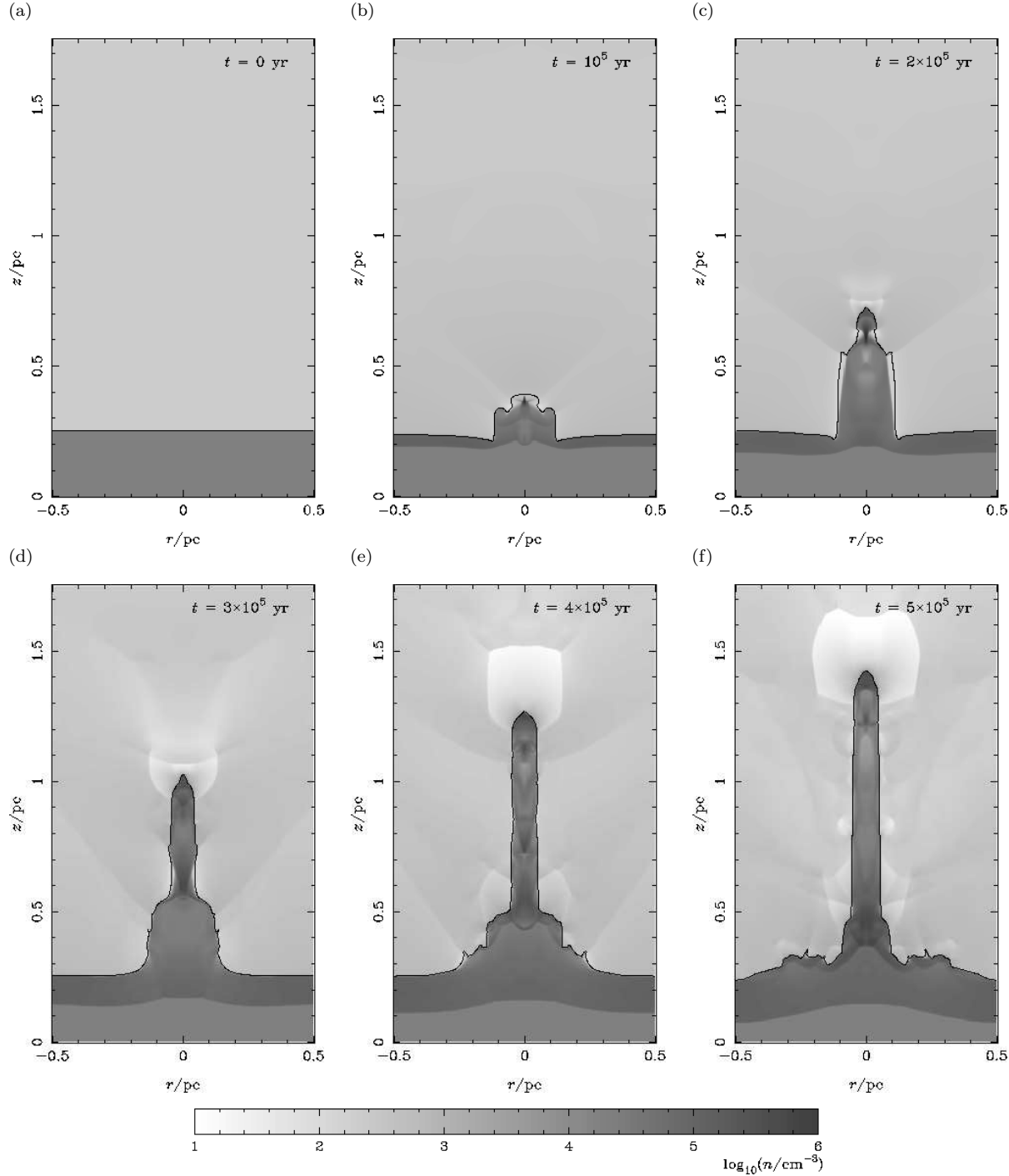


Figure 7. Greyscale plots of log density for Case III, stationary, initially uniform gas with 10 per cent decrease in ionizing radiation field within a 0.125 pc radius of the axis. The plots are shown at (a) initial conditions, (b) 1×10^5 yr, (c) 2×10^5 yr, (d) 3×10^5 yr, (e) 4×10^5 yr, and (f) 5×10^5 yr after the start of the simulation. The density range calibration is shown in the colour bar.

fuse emission and the multiple ionizing stars (Pavlakis et al. 2001).

This model seems similar to that discussed by White et al. However, it will be noted that by the time the ionization front reaches the dense clump, it interacts with the reflection of the main shock front from the dense core, rather than driving a separate shock itself. Shocks are al-

ways present within the solution, but are a characteristic of the dynamically disturbed nature of the flow.

Here we have *imposed* a separate potential, rather than calculating the gravity self-consistently, primarily as a computational convenience. However, it should be noted that in the Eagle columns, a reasonable fraction of the gravitational potential may be generated by protostellar clumps which have effectively decoupled from the flow. The small

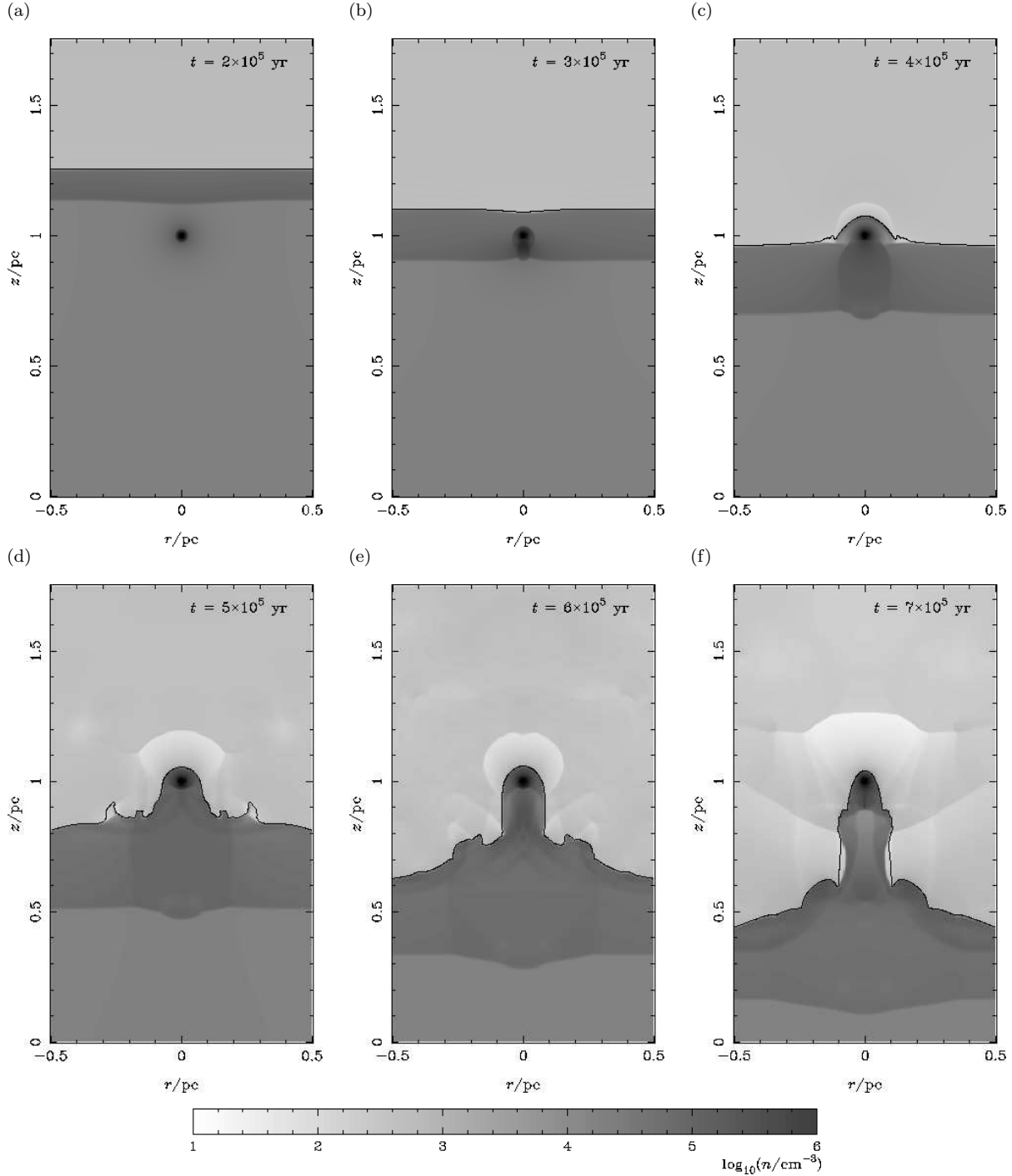


Figure 8. Greyscale plots of log density for Case IV: stationary, initially uniform gas with a $30 M_{\odot}$ gravitational field applied. The plots are shown at (a) 2×10^5 yr, (b) 3×10^5 yr, (c) 4×10^5 yr, (d) 5×10^5 yr, (e) 6×10^5 yr, and (f) 7×10^5 yr after the start of the simulation. The density range calibration is shown in the colour bar.

smoothing radius means that the gravitational field could not be generated by the self-gravity of a stable isothermal molecular gas core. It is possible that protostellar cores may be formed from gravitational instabilities in the swept up gas shell (Francis & Whitworth, in preparation), or be present in the initial molecular cloud.

Note, however, that if the heads of the columns were formed from individual isothermal cores confined by self-

gravity, then these cores must have been surrounded by significantly hotter, less dense gas if the overall structure was not to be unstable to gravitational collapse. In this case, the source of the $\sim 10^4 \text{ cm}^{-3}$ gas in the column behind the column is unclear.

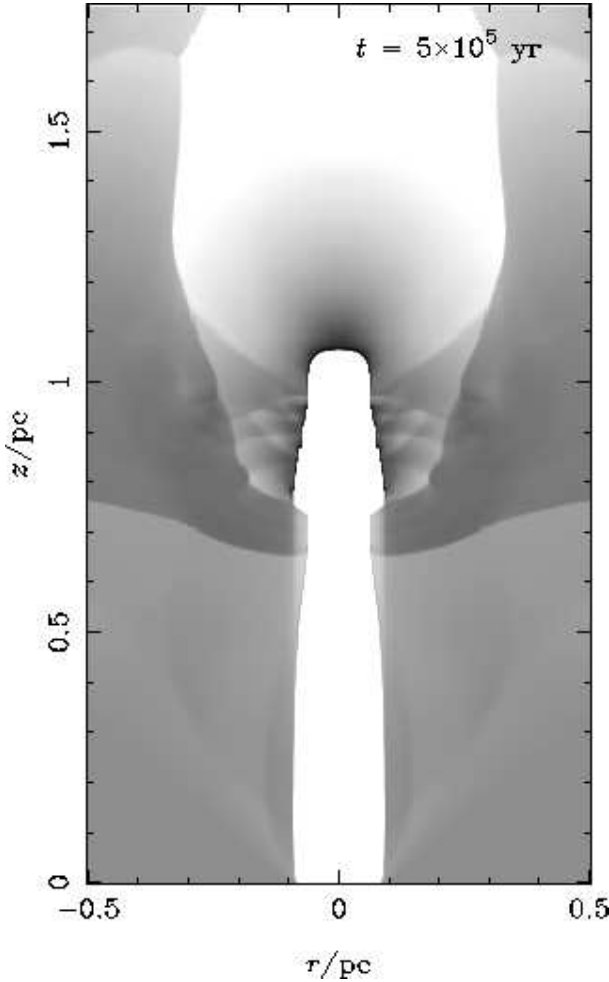


Figure 9. Greyscale plot of $\text{H}\alpha$ emission. The values are calculated for the simulation frame shown in Figure 5(f), 5×10^5 yr after the start of the simulation. The greyscale is linear, and saturates at an intermediate flux. Note that the emissivity in the symmetry plane is shown here, rather than the line-of-sight integral.

5.1 Discussion

In each of the cases presented in the present section, structures strikingly reminiscent of those observed by White et al. (1999) are maintained within the computational grid for periods of several 10^5 yr. The overall structures observed for models run for a range of similar parameters were broadly the same, suggesting that our results are not dependent on the details of our numerical or physical assumptions. This suggests that structures seen in M 16 are in a near-steady state, with the head of the column confined by the rocket effect at the front and by the ram pressure of the gas being swept up, by self-gravity, or a combination of the two. The structures can survive for several times 10^5 yr, longer than the shock crossing time of the head of the column, and similar to the dynamical age of M 16 as a whole. However, the influence of the symmetry axis on the stability of these columns means that this interpretation is tentative, until fully three-dimensional models are available.

In Figure 9, we show the $\text{H}\alpha$ emissivity expected from the gas within Case I after 5×10^5 yr from the start of the simulation, calculated as in Steffen et al. (1997). This image

shows the presence of bright rims and strong linear features in the flow away from the surface.

Since the structures appear to be close to equilibrium, the observations contain limited information about the mechanisms by which they formed: as we have shown, a variety of initial conditions can lead to very similar final structures. However, the observations seem not to *require* highly stratified density structures to have been present in the original molecular cloud. Indeed, it seems possible that the columns result from instabilities of the rim of a champagne-type expanding HII region (Tenorio-Tagle 1979; Bodenheimer et al. 1979). It is difficult to make substantial analytic progress in the study of such surface perturbations, as a result of the nonlocal nature of the system. As we have seen in the simulations, density enhancements resulting from fluctuations in the surface a significant time ago can result in long term variations in the ionizing flux incident on the surface a considerable distance from the original perturbation. While it is certainly true that the assumption of cylindrical symmetry enhances the variation of ionizing flux on the axis, it seems likely that the long lags between perturbation and response inherent in the system will in general lead to overstabilities of the flows, when studied on large scales.

The interpretation we have developed, however, has its own coincidental features. Most particularly, the mass of shocked molecular gas at the head of the columns is curiously close to the Jeans mass. There is no obvious dynamical reason for the mass of dense gas to settle on any particular value: indeed, we have seen the mass of dense gas to be highly variable in our simulations. A possible explanation for why the mass is close to the limit of collapse is that, in fact, the mass at the head increases as the column erodes, but once it reaches the limit of stability it collapses. The dense, self-gravitating globules produced will then no longer be subject to significant radiation or hydrodynamic forces, and can be left behind by the further photoevaporation of the column. In this manner, an ionization front can lead to stars forming in an episodic manner over a substantial period, compared to the one-off radiation-induced collapse of clumps which has been studied previously (Bok, as referred to by Oort 1954; Sandford et al. 1982; Bedijn & Tenorio-Tagle 1984; Bertoldi 1989). Note that the ionizing radiation incident on a clump will increase gradually when the main ionization front is of D-type, rather than suddenly as often assumed. The shock which precedes the IF may however result in a thin gas layer unstable to gravitational collapse (Elmegreen & Lada 1977; Whitworth et al. 1994) and may trigger the collapse of any pre-existing self-gravitating clumps (Megeath & Wilson 1997). To develop these ideas further requires models in which the self-gravity of the molecular gas is included.

6 CONCLUSIONS

In this paper, we have presented hydrodynamical models of the development of photoionized columns, which agree well with the observations of the columns in M 16. Our models contrast with the results of White et al., who interpret observations of the columns in M 16 as requiring that they have been exposed to the radiation field for less than 10^5 years, the dense material in the head of the column being a

gravitationally-bound condensation from the initial molecular cloud.

It remains to determine unambiguously how columns such as those in M 16 form, and how they evolve, if indeed there is any single mechanism. It seems likely, however, that these structures are often long lived components of the environment of massive stars, and of great importance in the formation of lower mass stars in these environments, and so they warrant further detailed study.

ACKNOWLEDGMENTS

The work of RJRW is supported by the PPARC through the award of an Advanced Fellowship. We would like to thank the referee, Matt Redman, for a helpful and constructive report.

REFERENCES

André P., 1996, *Mem.S.A.It.*, 67, 901
 Axford W.I., 1964, *ApJ*, 140, 112
 Bedijn P.J., Tenorio-Tagle G., 1984, *A&A*, 135, 81
 Bertoldi F., 1989, *ApJ*, 346, 735
 Bertoldi F., McKee C.F., 1990, *ApJ*, 354, 529
 Bertoldi F., McKee C.F., Klein R.I., 1993, in 'Massive Stars: Their Lives in the Interstellar Medium', *ASP Conf. Ser.* 35, Cassinelli J.P., Churchwell E.B., eds., 129
 Bertoldi F., Draine B.T., 1996, *ApJ*, 458, 222
 Bodenheimer P., Tenorio-Tagle G., Yorke H.W., 1979, *ApJ*, 233, 85
 Cantó J., Raga A.C., Steffen W., Shapiro P.R., 1998, *ApJ*, 502, 695
 Elmegreen B.J., Lada C.J., 1977, *ApJ*, 214, 725
 Falle S.A.E.G., 1991, *MNRAS*, 250, 581
 García-Segura G., Franco J., 1996, *ApJ*, 469, 171
 Giuliani J.L., 1979, *ApJ*, 233, 280
 Henney W.J., Arthur S.J., 1998, *AJ*, 116, 322
 Hester J.J., et al., 1996, *AJ*, 111, 2349
 Kahn F.D., 1958, *Rev. Mod. Phys.*, 30, 1058
 Lefloch B., Lazareff B., 1994, *A&A*, 289, 559
 Lefloch B., Lazareff B., Castets A., 1997, *A&A*, 324, 249
 Levenson N.A., Graham J.R., McLean I.S., Becklin E.E., Figer D.F., Gilbert A.M., Larkin J.E., Teplitz H.I., Wilcox M.K., 2000, *ApJL*, 533, L53
 Megeath S.T., Wilson T.L., 1997, *AJ*, 114, 1106
 Mellemma G., Raga A.C., Cantó J., Lundqvist P., Balick B., Steffen W., Noriega-Crespo A., 1998, *A&A*, 331, 335
 Nelson R.P., Langer W.D., 1997, *ApJ*, 482, 796
 Oort J.H., 1954, *BAN*, 12, 177
 Oort J.H., Spitzer L., 1954, *ApJ*, 121, 6
 Pavlakis K.G., Williams R.J.R., Dyson J.E., Falle S.A.E.G., Hartquist T.W., 2001, *A&A*, in press
 Pound M.W., 1998, *ApJL*, 493, L113
 Rubin R.H., 1968, *ApJ*, 153, 761
 Sandford M.T., Whitaker R.W., Klein R.I., 1982, *ApJ*, 260, 183
 Sankrit R., Hester J.J., 2000, *ApJ*, 535, 847
 Steffen W., Gómez J.L., Williams R.J.R., Raga A.C., Pedlar A., 1997, *MNRAS*, 286, 1032
 Sysoev N.E., 1997, *Astron. Lett.*, 23, 409
 Tenorio-Tagle G., 1979, *A&A*, 71, 59
 Vandervoort P.O., 1962, *ApJ*, 135, 212
 White G.J., et al., 1999, *A&A*, 342, 233
 Whitworth A.P., Bhattacharjee A.S., Chapman S.J., Disney M.J., Turner J.A., 1994, *MNRAS*, 268, 291

Williams R.J.R., 1999, *MNRAS*, 310, 789